Ytterbium-doped oxyfluoride nano-glass-ceramic fibers for laser cooling

Kummara Venkata Krishnaiah, Yannick Ledemi, Cécile Genevois, Emmanuel Véron, Xavier Sauvage, Steeve Morency, Elton Soares de Lima Filho, Galina Nemova, Mathieu Allix, Younes Messaddeq, et al.

Research Article | Vol. 7, No. 6 | 1 Jun 2017 | OPTICAL MATERIALS EXPRESS 1980
Optical Materials EXPRESS

Ytterbium-doped oxyfluoride nano-glass-ceramic fibers for laser cooling

KUMMARA VENKATA KRISHNAIAH,[1,2,*] YANNICK LEDEMI,[2] CÉCILE GENEVOIS,[3] EMMANUEL VERON,[3] XAVIER SAUVAGE,[4] STEEVE MORENCY,[2] ELTON SOARES DE LIMA FILHO,[1,2] GALINA NEMOVA,[1] MATHIEU ALLIX,[3] YOUNES MESSADDEQ,[2] AND RAMAN KASHYAP[1,5]

[1]*Department of Engineering Physics, Polytechnique de Montréal, P.O. Box 6079, Station Centre-ville, Montréal H3C 3A7, Canada*
[2]*Centre d'Optique, Photonique et Laser, 2375 Rue de la Terrasse, Université Laval, Québec G1V 0A6, Canada*
[3]*Conditions Extrêmes et Matériaux: Haute Température et Irradiation, CEMHTI-CNRS UPR3079, 1D avenue de la Recherche Scientifique, 45071, Orléans Cedex 2, France*
[4]*Normandie Université, UNIROUEN, INSA Rouen, CNRS, Physics of Materials Group, 76000 Rouen, France*
[5]*Department of Electrical Engineering, Polytechnique de Montréal, P.O. Box 6079, Station Centre-ville, Montréal H3C 3A7, Canada*
[*]*kvkphd84@gmail.com*

Abstract: Ytterbium (Yb^{3+})-doped oxyfluoride SiO_2-Al_2O_3-CdF_2-PbF_2-YF_3 glass and nano-glass-ceramic (i.e. glass-ceramics containing nanocrystals) single-index optical fibers were fabricated using two methods: by traditional glass preform drawing and by the crucible technique ('direct-melt process'). The latter technique permitted the fabrication of perfectly vitreous optical fibers (of about 200 µm diameter), leading subsequently to the fabrication of nano glass-ceramic fibers by a well-controlled heat-treatment process above the glass transition temperature. Structural characterizations have (i) confirmed the vitreous state (absence of crystals) of the glass preforms and the glass fiber obtained from the 'direct-melt process' and, (ii) evidenced the formation of $Pb_{1-x-y-z}Cd_xY_yYb_zF_2$ ($x + y + z \approx 0.3$-0.4) fluorite nanocrystals in the final glass-ceramic fibers. In particular, the nanocrystal size was found to be rather homogenous and smaller than 10 nm from TEM measurements for the nano-glass-ceramic fibers produced by controlled crystallization. The absolute photoluminescence quantum efficiency, mean fluorescence wavelength and anti-Stokes fluorescence of the Yb^{3+}-doped fibers were measured upon laser excitation at wavelengths of 940 nm, 975 nm and 1030 nm, respectively. As expected, higher photoluminescence quantum yield in the near infrared (0.95, close to unity) was obtained for the nano-glass-ceramic fiber when compared with the glass-fiber. Theoretical calculations were also carried out, showing that optical refrigeration would be achievable from these chemically stable and durable nano-glass-ceramic fibers provided that 95% (segregation ratio) of Yb^{3+} ions are incorporated into the fluorite nanocrystals.

OCIS codes: (160.2750) Glass and other amorphous materials; (160.4760) Optical properties; (160.5690) Rare-earth doped materials; (160.2290) Fiber materials; Spectroscopy, fluorescence and luminescence (300.6280); 160.4236 Nanomaterials

References

1. Y. H. Wang and J. Ohwaki, "New transparent vitroceramics codoped with Er^{3+} and Yb^{3+} for efficient frequency up-conversion," Appl. Phys. Lett. **63**(24), 3268–3270 (1993).
2. M. Ferrari and G. C. Righini, "Glass-Ceramic Materials for Guided-Wave Optics," Int. J. Appl. Glass Sci. **6**(3), 240–248 (2015).
3. S. Fujita and S. Tanabe, "Glass-Ceramics and Solid-State Lighting," Int. J. Appl. Glass Sci. **6**(4), 356–363 (2015).
4. C. Liu and J. Heo, "Nanocrystal Formation in Glasses Controlled by Rare Earth Ions," Int. J. Appl. Glass Sci. **5**(2), 104–113 (2014).

#285975 https://doi.org/10.1364/OME.7.001980
Journal © 2017 Received 2 Feb 2017; revised 28 Apr 2017; accepted 28 Apr 2017; published 18 May 2017

Optical Materials EXPRESS

5. A. J. Stevenson, H. Serier-Brault, P. Gredin, and M. Mortier, "Fluoride materials for optical applications: Single crystals, ceramics, glasses, and glass-ceramics," J. Fluor. Chem. **132**(12), 1165–1173 (2011).
6. P. P. Fedorov, A. A. Luginina, and A. I. Popov, "Transparent oxyfluoride glass ceramics," J. Fluor. Chem. **172**, 22–50 (2015).
7. Z. Fang, S. Zheng, W. Peng, H. Zhang, Z. Ma, G. Dong, S. Zhou, D. Chen, and J. Qiu, "Ni($^{2+}$) doped glass ceramic fiber fabricated by melt-in-tube method and successive heat treatment," Opt. Express **23**(22), 28258–28263 (2015).
8. Z. Fang, S. Zheng, W. Peng, H. Zhang, Z. Ma, S. Zhou, D. Chen, and J. Qiu, "Fabrication and Characterization of Glass-Ceramic Fiber-Containing Cr^{3+}-Doped $ZnAl_2O_4$ Nanocrystals," J. Am. Ceram. Soc. **98**(9), 2772–2775 (2015).
9. Y. Teng, K. Sharafudeen, S. F. Zhou, and J. R. Qiu, "Glass-ceramics for photonic devices," J. Ceram. Soc. Jpn. **120**(1407), 458–466 (2012).
10. S. Chenu, E. Veron, C. Genevois, A. Garcia, G. Matzen, and M. Allix, "Long-lasting luminescent $ZnGa_2O_4$:Cr^{3+} transparent glass-ceramics," J. Mater. Chem. C Mater. Opt. Electron. Devices **2**(46), 10002–10010 (2014).
11. Y. Ledemi, A. A. Trudel, V. A. G. Rivera, S. Chenu, E. Veron, L. A. Nunes, M. Allix, and Y. Messaddeq, "White light and multicolor emission tuning in triply doped Yb^{3+}/Tm^{3+}/Er^{3+} novel fluoro-phosphate transparent glass-ceramics," J. Mater. Chem. C Mater. Opt. Electron. Devices **2**(25), 5046–5056 (2014).
12. C. Rüssel, "Nanocrystallization of CaF_2 from Na_2O/K_2O/CaO/CaF_2/Al_2O_3/SiO_2 glasses," Chem. Mater. **17**(23), 5843–5847 (2005).
13. G. H. Beall and L. R. Pinckney, "Nanophase glass-ceramics," J. Am. Ceram. Soc. **82**(1), 5–16 (1999).
14. R. I. Epstein, M. I. Buchwald, B. C. Edwards, T. R. Gosnell, and C. E. Mungan, "Observation of laser-induced fluorescent cooling of a solid," Nature **377**, 500–503 (1995).
15. M. Sheik-Bahae and R. I. Epstein, "Laser cooling of solids," Laser Photonics Rev. **3**(1-2), 67–84 (2009).
16. A. J. Garcia-Adeva, R. Balda, and J. Fernandez, "Laser cooling of Er^{3+}-doped low-phonon materials: Current status and outlook," Opt. Mater. **31**(7), 1075–1081 (2009).
17. E. S. Filho, K. V. Krishnaiah, Y. Ledemi, Y. J. Yu, Y. Messaddeq, G. Nemova, and R. Kashyap, "Ytterbium-doped glass-ceramics for optical refrigeration," Opt. Express **23**(4), 4630–4640 (2015).
18. M. P. Hehlen, M. Sheik-Bahae, R. I. Epstein, S. D. Melgaard, and D. V. Seletskiy, "Materials for Optical Cryocoolers," J. Mater. Chem. C Mater. Opt. Electron. Devices **1**(45), 7471–7478 (2013).
19. G. M. Tao, H. Ebendorff-Heidepriem, A. M. Stolyarov, S. Danto, J. V. Badding, Y. Fink, J. Ballato, and A. F. Abouraddy, "Infrared fibers," Adv. Opt. Photonics **7**(2), 379–458 (2015).
20. H.-W. Chen, J. Lim, S.-W. Huang, D. N. Schimpf, F. X. Kärtner, and G. Chang, "Optimization of femtosecond Yb-doped fiber amplifiers for high-quality pulse compression," Opt. Express **20**(27), 28672–28682 (2012).
21. Y. Joeng, Y. Kim, A. Liem, K. Moerl, S. Hoefer, A. Tuennermann, and K. Oh, "Q-switching of Yb^{3+}-doped fiber laser using a novel micro-optical waveguide on microactuating platform light modulator," Opt. Express **13**(25), 10302–10309 (2005).
22. M. Bashkansky, M. Duncan, L. Goldberg, J. Koplow, and J. Reintjes, "Characteristics of a Yb-doped superfluorescent fiber source for use in optical coherence tomography," Opt. Express **3**(8), 305–310 (1998).
23. G. Nemova and R. Kashyap, "Fiber amplifier with integrated optical cooler," J. Opt. Soc. Am. B **26**(12), 2237–2241 (2009).
24. D. Dorosz, J. Dorosz, A. Zajac, J. Zmojda, and M. Kochanowicz, "Active optical fibres for application in laser and broadband ASE sources," Bull. Pol. Acad. Sci. Tech. Sci. **60**(4), 673–682 (2012).
25. Q. Sheng, X. Wang, and D. Chen, "Enhanced broadband near-infrared luminescence and its origin in Yb/Bi co-doped borophosphate glasses and fibers," J. Quant. Spectrosc. Radiat. Transf. **141**, 9–13 (2014).
26. S. W. Moore, T. Barnett, T. A. Reichardt, and R. L. Farrow, "Optical properties of Yb^{3+}-doped fibers and fiber lasers at high temperature," Opt. Commun. **284**(24), 5774–5780 (2011).
27. M. C. Paul, S. Bysakh, S. Das, S. K. Bhadra, M. Pal, S. Yoo, M. P. Kalita, A. J. Boyland, and J. K. Sahu, "Yb_2O_3-doped YAG nano-crystallites in silica-based core glass matrix of optical fiber preform," Materials Science and Engineering B-Advanced Functional Solid-State Materials **175**(2), 108–119 (2010).
28. P. A. Tick, "Are low-loss glass ceramic optical waveguides possible?" Opt. Lett. **23**(24), 1904–1905 (1998).
29. B. N. Samson, P. A. Tick, and N. F. Borrelli, "Efficient neodymium-doped glass-ceramic fiber laser and amplifier," Opt. Lett. **26**(3), 145–147 (2001).
30. P. A. Tick, N. F. Borrelli, and I. M. Reaney, "The relationship between structure and transparency in glass-ceramic materials," Opt. Mater. **15**(1), 81–91 (2000).
31. M. Mortier, P. Goldner, C. Chateau, and M. Genotelle, "Erbium doped glass-ceramics: concentration effect on crystal structure and energy transfer between active ions," J. Alloys Compd. **323-324**, 245–249 (2001).
32. G. Dantelle, M. Mortier, G. Patriarche, and D. Vivien, "Er^{3+}-doped PbF_2: Comparison between nanocrystals in glass-ceramics and bulk single crystals," J. Solid State Chem. **179**(7), 1995–2003 (2006).
33. G. Dantelle, M. Mortier, D. Vivien, and G. Patriarche, "Nucleation efficiency of erbium and ytterbium fluorides in transparent oxyfluoride glass-ceramics," J. Mater. Res. **20**(02), 472–481 (2005).
34. K. V. Krishnaiah, E. S. de Lima Filho, Y. Ledemi, G. Nemova, Y. Messaddeq, and R. Kashyap, "Development of ytterbium-doped oxyfluoride glasses for laser cooling applications," Sci. Rep. **6**(1), 21905 (2016).
35. G. Nemova, *Laser Cooling: Fundamental Properties and Application*, G. Nemova, ed. (Pan Stanford Publishing, 2016), chapter 2.
36. G. Nemova and R. Kashyap, "Laser cooling with Tm^{3+}-doped oxy-fluoride glass ceramic," J. Opt. Soc. Am. B **29**(11), 3034–3038 (2012).
37. P. Zhang, J. Yin, B. Zhang, L. Zhang, J. Hong, J. He, and Y. Hang, "Intense 2.8 μm emission of Ho^{3+} doped PbF_2 single crystal," Opt. Lett. **39**(13), 3942–3945 (2014).

Optical Materials EXPRESS

38. Y. Kawamoto, R. Kanno, and J. Qiu, "Upconversion luminescence of Er^{3+} in transparent SiO_2-PbF_2-ErF_3 glass ceramics," J. Mater. Sci. **33**(1), 63–67 (1998).
39. G. Nemova and R. Kashyap, "Temperature distribution in laser-cooled rare-earth doped solid-state samples," J. Opt. Soc. Am. B **27**(12), 2460–2464 (2010).
40. P. Yan, M. Gong, C. Li, P. Ou, and A. Xu, "Distributed pumping multifiber series fiber laser," Opt. Express **13**(7), 2699–2706 (2005).
41. S. Chenu, E. Veron, C. Genevois, G. Matzen, T. Cardinal, A. Etienne, D. Massiot, and M. Allix, "Tuneable Nanostructuring of Highly Transparent Zinc Gallogermanate Glasses and Glass-Ceramics," Advanced Optical Materials **2**(4), 364–372 (2014).
42. R. W. Cheary and A. Coelho, "A fundamental parameters approach to x-ray line-profile fitting," J. Appl. Cryst. **25**(2), 109–121 (1992).
43. N. H. Kolderup, "Crystal structure of fluorides of divalent metals," Mineralogical Abstracts **3**, 340 (1924).
44. H. M. Haendler and W. J. Bernard, "The reaction of fluorine with cadmium and some of its binary compounds - the crystal structure, density and melting point of cadmium fluoride," J. Am. Chem. Soc. **73**(11), 5218–5219 (1951).
45. R. D. Shannon, "Revised effective ionic-radii and systematic studies of interatomic distances in halides and chalcogenides," Acta Crystallogr. A **32**(5), 751–767 (1976).
46. T. Höche, C. Patzig, T. Gemming, R. Wurth, C. Russel, and I. Avramov, "Temporal Evolution of Diffusion Barriers Surrounding $ZrTiO_4$ Nuclei in Lithia Aluminosilicate Glass-Ceramics," Cryst. Growth Des. **12**(3), 1556–1563 (2012).
47. D. V. Seletskiy, M. P. Hehlen, R. I. Epstein, and M. Sheik-Bahae, "Cryogenic optical refrigeration," Adv. Opt. Photonics **4**(1), 78–107 (2012).
48. F. Auzel, D. Meichenin, F. Pelle, and P. Goldner, "Cooperative luminescence as a defining process for RE-ions clustering in glasses and crystals," Opt. Mater. **4**(1), 35–41 (1994).
49. F. Auzel, "Upconversion and anti-Stokes processes with f and d ions in solids," Chem. Rev. **104**(1), 139–174 (2004).
50. G. Nemova and R. Kashyap, "Optimization of optical refrigeration in Yb^{3+}: YAG samples," J. Lumin. **164**, 99–104 (2015).

1. Introduction

In 1993, Wang and Ohwaki reported for the first time enhanced luminescence properties in novel Er^{3+} and Yb^{3+}-doped transparent oxyfluoride SiO_2-Al_2O_3-CdF_2-PbF_2 glass-ceramics (GCs) compared to their parent glasses [1]. GCs are composite materials which are composed of crystals homogeneously distributed in a vitreous matrix. The most common route to synthesize GCs consists of heat-treating a parent glass to enable controlled crystal growth. Nonetheless, alternative fabrication methods are also emerging since a decade, owing to the large interest aroused by transparent GCs for advanced applications in optics and photonics [2–12]. By tailoring both the crystal size and/or the refractive index difference between crystalline and vitreous phases during the crystallization process, it is actually possible to minimize light scattering and ensure optical transparency of the GC in the spectral region of interest. According to the Rayleigh-Gans theory about particle scattering, the crystal size has to be much smaller than the incident light wavelength while the refractive index difference has to be minimized to achieve optical transparency [13]. As the crystals present in such transparent glass-ceramics must exhibit a nanometer scale (below 100 nm), these materials are usually called nano-glass-ceramics.

Laser cooling of solids was first demonstrated under vacuum by Epstein *et al*. in an Yb^{3+}-doped fluoride ZBLANP glass [14]. A temperature decrease of 0.3 K below room temperature was achieved by excitation with a 1010 nm laser. Since then, efforts are continuing to develop low cost and efficient solid-state optical coolers owing to the possibility of vibration-free refrigeration systems [15]. For instance, optical cooling was recently demonstrated under vacuum and ambient atmosphere in single crystals doped with Yb^{3+}, Tm^{3+} and Er^{3+} ions whose spectral transmission, background absorption and photoluminescence quantum yield (PLQY) were carefully studied [16–18]. In our earlier studies, we showed the potential of using Yb^{3+}-doped bulk glasses (G) and GCs belonging to the SiO_2-Al_2O_3-CdF_2-PbF_2-YF_3 system (derived from the discovery by Wang and Ohwaki [1]) for laser cooling applications based on their PLQYs being close to unity [17]. Indeed, it was previously demonstrated that a PLQY close to unity is favorable for achieving laser cooling in rare earth ions (*RE*) doped materials [14].

Optical Materials EXPRESS

Developing solid-state optical coolers in the form of fibers is of major interest. Optical fibers (with diameter of 200 μm and below) are well-known for their light-guiding capabilities, high mechanical flexibility and/or large surface area to volume ratio making them materials of first choice for the development of compact fiber lasers, sensors, etc [19]. *RE* ions and more particularly ytterbium (Yb^{3+})-doped optical fibers have been utilized for applications in amplifiers [20], lasers [21], and for superfluorescence [22], integrated optical coolers (theoretical approximation) [23] and broadband amplified spontaneous emission (ASE) [24] sources, to name a few. Yb^{3+} ion can also act as a sensitizer by transferring absorbed energy and broadening the Bi^{+} and Bi^{2+} near infrared emission in borophosphate glasses and fibers upon 975 nm wavelength laser excitation, for instance [25]. The optical properties of Yb^{3+}-doped silica fibers, including their absorption coefficient, emission cross-section, fluorescence lifetime and temperature dependence, have been reported [26]. Silicate-based optical preforms containing Yb^{3+}-doped yttrium aluminum garnet (YAG) nano-crystals were also prepared by the MCVD technique and tested to produce optical fibers [27]. Yb^{3+}-doped nano-glass-ceramic optical fibers (i.e. glass optical fiber containing nanocrystals) may therefore offer advantageous properties over conventional glass fibers such as enhanced optical, mechanical and/or thermal properties, improved resistance to high power laser excitation, etc. Actually, such glass-ceramic optical fibers were already developed about 15 years ago by Corning [28–30]. Indeed, Tick *et al*. [28] first reported on the fabrication of relatively low-loss (750 dB/km at 1350 nm) Tm^{3+}-doped GC optical fiber based on the SiO_2-Al_2O_3-CdF_2-PbF_2 system. Later, they also reported on Nd^{3+}-doped GC fiber laser and amplifier from the same glass system [29]. They demonstrated that appropriate heat-treatments at different temperatures ranging from 440 to 470 °C of the oxyfluoride glass fiber can lead to the formation of glass-ceramic fiber with crystal size lower than 10 nm while maintaining a relatively low level of scattering losses [30]. Although they were not able to determine the crystal phase directly from the fiber structural characterization, they compared their results with a PbF_2-CdF_2-YF_3 bulk crystal and proposed the $60PbF_2$-$20CdF_2$-$20YF_3$ crystal composition [30]. On the other hand, the favored incorporation of *RE* ions into lead fluoride based nanocrystals in transparent glass-ceramics was also largely investigated by Mortier *et al*. [31–33].

The aim of the present study is to take advantage of both the ability of the lead-cadmium oxyfluoride glass system to form transparent and durable nano-glass-ceramics with promising optical properties and their underexplored potential to be drawn into optical fibers in order to propose a new fiber material for laser cooling applications. For such purpose, several requirements have to be fulfilled: (i) high photoluminescence quantum yield (close to unity), low background absorption (order of $\sim 10^{-4}$ cm^{-1}) and low phonon energy and; (ii) crystals size lower than 20 nm with a narrow size distribution and uniform dispersion with a suitable inter-particle spacing within the glassy matrix, no secondary crystal phases, etc. We report here for the first time, to the best of our knowledge, on the preparation and characterization of 2 mol% Yb^{3+}-doped SiO_2-Al_2O_3-CdF_2-PbF_2-YF_3 glass (G) and nano-glass-ceramic (GC) optical fibers with uniform crystal size for future laser cooling applications. Two methods were implemented: (i) fiber drawing from an optical glass preform and (ii) fiber drawing by using the crucible technique ('direct-melt process'). Special attention was given to monitor the vitreous and crystalline phases by using X-ray diffraction and transmission electron microscope analyses. The PLQY and mean fluorescence wavelength of the fibers were determined by photoluminescence measurements carried out with and without an integrating sphere, respectively. Finally, the advantages offered by the GC-fiber over the G-fiber are discussed in the light of laser cooling applications.

2. Experimental details

2.1. Glass preparation

As mentioned above, the first method implemented to produce optical fibers consisted of drawing an optical glass preform in our home-made 7 m height fiber drawing tower. First,

Optical Materials EXPRESS

$30SiO_2–15Al_2O_3–27CdF_2–22PbF_2–4YF_3–2YbF_3$ (mol%) oxyfluoride glass rods of about 30 g were prepared by the conventional melt-quenching technique. High purity commercial starting materials (99.99%) were mixed in an agate mortar to obtain a homogeneous mixture which was then loaded in a platinum crucible. After melting and fining at 1100°C for 1h in an induction furnace under dry nitrogen gas flow (2 L/min), the glass was cast into a stainless steel mold which was preheated at 370°C (~40°C below the glass transition temperature). Annealing of the preform was subsequently carried out at the same temperature for 5h before cooling down to room temperature to remove any residual internal stresses. Finally, glass rods of 10 mm diameter and ~50 mm length were carefully polished with a home-designed preform polishing system to produce single-index glass preforms for further fiber drawing.

2.2. Optical fiber fabrication

2.2.1. By drawing from the glass preform

In this first method, the glass preforms previously prepared are mounted in the drawing induction furnace of the fiber tower and rapidly heated up to 550°C under dry N_2 flow (5 L/min). After attaining its softening point, the glass preform is stretched with optimized parameters including furnace temperature, preform feeding speed and tension applied to the fiber. The diameter of the produced fiber is therefore finely tailored to be about 200 µm. No protective coating was applied to the fiber as no sensitivity to moisture was observed for this oxyfluoride material. In such a method, it is worth mentioning that optical fibers are produced by reheating the glass preforms well above their glass transition temperature, (T_g = 410 °C) [34]. Special attention has thus to be paid here as the material under study is prone to nanocrystallization at temperatures above T_g, as it will be discussed in the next section. The obtained optical fibers are labeled as GC-fiber1 as they are considered to be already partly crystallized which will be demonstrated in the results section.

2.2.2. By the crucible technique ('direct-melt process')

A second approach was also used to produce the SiO_2-Al_2O_3-CdF_2-PbF_2-YF_3:YbF_3 optical fibers. It consisted of drawing the fiber directly from the glass melt. Contrary to the first method, the crucible technique enables the fabrication fiber without the reheating step. The optical fiber is indeed produced after appropriate adjustment of the glass viscosity from its molten state, i.e. after lowering the temperature of the melt. In practice, the crucible containing the molten glass at high temperature (1100 °C) is first removed from the induction furnace and allowed to cool in ambient air down to a temperature of ~800-900°C (measured by a pyrometer) to decrease the glass viscosity. Fibers of ~1 m length and ~200 µm diameter are then manually drawn (in ambient air) from the viscous glass with the help of a silica rod dipped into the crucible. Through this technique, one expects first to limit the formation of nanocrystals by getting rid of the reheating process (characteristic of the first method) and second, to achieve sufficient cooling rate to obtain glass fibers (G-fiber2) free of nanocrystals (which could be generated during glass cooling).

In a second step, Yb^{3+}-doped nano-glass-ceramic fibers (GC-fiber2) with controlled crystallite size are obtained from the G-fiber2 by a simple crystallization heat-treatment at 460°C (~T_g + 50 °C) for 20h and subsequent cooling to room temperature.

2.3. Fiber characterization

The X-ray powder diffraction (XRPD) patterns were collected over the 15–70° 2θ range with a 0.0245° step (4 s per step counting time) on an X-ray Bruker D8 Advance ($CuK\alpha_{12}$ radiation) equipped with a Vantec-1 linear detector. Transmission electron microscope (TEM) imaging was carried out using a Philips CM20 microscope. The STEM images and elemental compositions were obtained using a JEOL ARM200F FEG microscope operating at 200kV and equipped with a spherical aberration corrector on the probe and an Oxford Instrument EDS (Energy Dispersive Spectroscopy) system. Scanning transmission electron microscopy – high angle annular dark field (STEM-HAADF) images were acquired in the angle range of

Optical Materials EXPRESS

50-180mrad with an 8 cm camera length and a 0.1 nm probe size. Elemental compositions were determined by STEM-EDX using a similar 0.1 nm probe size. The samples were prepared in two different ways. First, some parts of the G-fiber2 were crushed in ethanol and a drop of the solution containing a small amount of material in suspension was deposited onto a carbon-coated copper grid. Then, for the GC-fiber2, a specific sample preparation was developed to observe the nanocrystals. A few pieces of 2 mm long fibers were laid parallel to each other and glued to obtain a planar fiber network. The resulting network was then mechanically polished on both sides, using inlaid diamond discs and a tripod, until a 50 µm thickness. The foil was finally thinned by argon ion bombardment (PIPS) to obtain sufficiently thin areas (tens of nm) to be observed by TEM. For the EDS analysis, a GC-fiber2 sample was specifically prepared. During the mechanical polishing with a tripod and inlaid diamond discs, a tilt was imposed in order to form a bevel on one side of the sample. Very thin areas were thus obtained without using final argon ion milling (PIPS, Precision Ion Polishing System - Gatan) which can sometimes induce some bombardment defaults.

Photoluminescence measurements were performed by exciting at a wavelength of 975 nm the fibers under test placed on a xyz-stage in a grooved glass slide with a microscope objective (0.6 NA, × 60) to achieve light coupling into the fiber. Luminescence was collected from the fiber output with a multimode fiber (200 µm diameter, 0.22 NA) coupled to an optical spectrum analyzer (OSA). Absolute photoluminescence quantum yield (PLQY) of the fiber was measured upon 940 nm laser excitation from a Ti:sapphire laser in an integrating sphere (ISp) of 2 inches internal diameter and an OSA. Anti-Stokes fluorescence was measured with an OSA upon laser excitation of the fibers at 1040 nm. The up conversion spectra were obtained by exciting with a 975 nm laser while emission was detected with a compact CCD spectrometer (Thorlabs CCS100).

3. Laser cooling theory

The cooling power arises in a fluorescent sample with very high (>98.5%) quantum efficiency (QE) if the power of the radiated photons exceeds the power of absorbed ones as a result of phonon annihilation. The laser cooling process based on anti-Stokes fluorescence can be realized in different systems, such as *RE*-doped low phonon energy glasses and crystals, direct band gap semiconductors and so on. The laser cooling process in *RE*-doped solids can be described with rate equations [35]. If a laser cooled sample is placed in a vacuum chamber with the walls at room temperature, T_r, the final equilibrium temperature of the sample, T_s, can be estimated following the Stefan-Boltzmann law [35, 36]:

$$V(P_{cool} - P_{heat}) = \varepsilon\sigma_B S(T_r^4 - T_s^4), \quad (1)$$

where P_{cool} and P_{heat} are the cooling and heating powers, respectively, generated in a sample with the volume V and the total surface area S. ε is the emissivity of the sample and $\sigma_B = 5.67 \times 10^{-12}$ W·cm^{-2}·K^{-4} is the Stefan-Boltzmann constant.

Oxyfluoride GC materials possess unique properties, which can be advantageous for laser cooling applications. Oxyfluoride GCs provide a low phonon energy fluoride crystalline environment to Yb^{3+} ions involved in the cooling or lasing cycles while retaining the chemical durability, the mechanical resistance and the ease of shaping of the silicate-based glassy network. Indeed, the phonon energy in lead fluoride based nanocrystals is very low (only ~250 cm^{-1}) [37] in comparison to that of high phonon silica glass (~1100 cm^{-1}) [38]. The low phonon energy of nanocrystals is a source of a significant increase in the quantum efficiency [35] of Yb^{3+} ions doped in crystalline environment in oxyfluoride GCs. Moreover, it is worth mentioning that low phonon crystals have some undisputable advantages over low phonon glasses for laser cooling [35]. Indeed, the structural disorder in glass materials is a source of inhomogeneous broadening of the absorption and emission bands, which is essentially independent of temperature. Contrary to glasses, inhomogeneous broadening in crystals is negligible and the spectral bandwidth is dominated by homogenous broadening. It

Optical Materials EXPRESS

scales as T^2 in the temperature range of 10-300K maintaining a higher peak absorption coefficient in crystals than in glasses.

Using Eq. (1), one can estimate a final achievable temperature of the sample as a function of the pump power for different parameters of Yb^{3+} doped GC fiber samples. It is important to emphasize that the configuration of the pump is very important for a cryocooler design, since the pump density distribution in a laser cooled sample is dependent on the temperature distribution in a laser cooled sample. We investigated the problem of the temperature gradient in laser cooled cylindrical samples in Ref [39]. For a long fiber with a large diameter, the temperature will change slightly along the radius as well as along the length of the fiber, since the pump power intensity decreases along its length of the fiber because of light absorption by active ions. The configuration of a pump source providing uniform pump power distribution along the length of the fiber must be considered for optimizing an optical cryocooler design. A side pumped fiber or a fiber pumped at both ends can be considered as a solution to this problem. We do not take into account the decrease in the pump power with the length of the sample, since in the case of laser cooling of solids it can be compensated for by a distributed pumping technique described in [40]. Indeed, the absorption cross sections of *RE* ions are very small in the long wavelength tail of the absorption spectrum, where the pump for laser cooling applications takes place. For example, for Yb^{3+} ion concentration $N_T = 5x10^8$ μm^{-3} only ~14% of the pump power will be absorbed by 1 cm of the sample. This decrease in the pump power can be compensated for by the distributed pumping technique. The recycling mechanism for the pump power such as a resonator must be a part of this scheme. Here we estimate the temperature of the SiO_2-Al_2O_3-CdF_2-PbF_2-YF_3:YbF_3 GC-fiber with a diameter of 200 μm uniformly side pumped along its length. The pump wavelength is λ_p = 1030 nm. The QE used in our simulations is 99.5%. The radiative lifetimes of Yb^{3+} ions in nanocrystals and glass matrix are 1.63 ms and 0.4 ms, respectively. The absorption and emission cross sections of Yb^{3+} ions in glass-ceramics (containing nanocrystals) are $3x10^{-14}$ μm^2 and $4.8x10^{-13}$ μm^2, respectively. The absorption cross section of Yb^{3+} ions in the glass matrix is $4x10^{-14}$ μm^2. The mean fluorescence wavelength of the active Yb^{3+} ions in GC fiber is 1010 nm. The hemispherical emissivity is 0.54. The temperature distribution across the diameter of this fiber can be considered as uniform. As one can see in Eq. (1) the final temperature of the sample does not depend on the length of the fiber with uniform pump power distribution. The most important parameters in the case of a GC-fiber sample are the segregation ratio of Yb^{3+} ions into the nanocrystals and *RE* ion concentration. Figure 1 illustrates the final temperature of the sample as a function of the pump power uniformly distributed along the length of the fiber for different segregation ratios of Yb^{3+} ions into the nanocrystals (Fig. 1(a)) and different ion concentrations (Fig. 1(b)). As the pump power increases the influence of both parameters on the final temperature of the sample increases. These parameters must be carefully controlled in GC-fiber samples for laser cooling applications. As may be seen from our simulations, a QE of 95% achieved in our samples can provide only heat mitigation. Improved QE (>0.985) and purification of samples are the most important parameters to achieving net laser cooling process.

Optical Materials EXPRESS

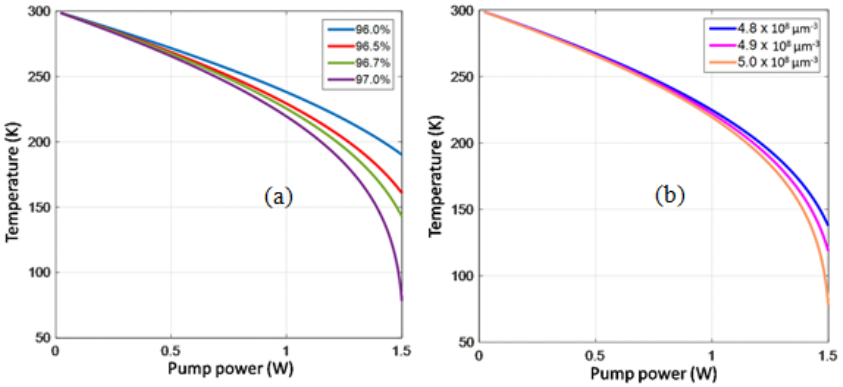

Fig. 1. Final calculated temperature of SiO_2-Al_2O_3-CdF_2-PbF_2-YF_3:YbF_3 GC-fiber samples with a diameter of 200 µm as a function of the uniformly distributed pump power. (a): Segregation ratios are 96.0%, 96.5%, 96.7%, 97.0%. (b): Yb^{3+}densities are 4.8 x 10^8 μm^{-3}, 4.9 x 10^8 μm^{-3}, 5.0 x 10^8 μm^{-3}.

4. Results and discussion

As described in the experimental method section, two types of fiber were produced: (i) the GC-fiber1 drawn from the glass preform for which crystallization is expected to occur during the fiber production and; (ii) the vitreous G-fiber2 fabricated by the crucible method from which the glass-ceramic GC-fiber2 is elaborated by subsequent thermal treatment. All the elaborated fibers show an excellent chemical durability (no reaction with moisture) and mechanical resistance, allowing their handling for characterization even without a protective coating after several months of storing in ambient conditions.

4.1. Structural characterization

The inset of Fig. 2 presents a photograph of the stretched drop corresponding to the very beginning of the fiber drawing process from the glass preform. This stage is then followed by the drawing of the GC-fiber1 under stabilized conditions and controlled diameter around 200 µm. It can be observed from the opalescence that an undesired and uncontrolled crystallization or nanophase separation which was measured to be in the range of 10-100 nm [41] of the material occurs here. The opalescence observed in glass-related materials after heat-treating above T_g (here during the fiber stretching at 550 °C) is usually attributed to the formation of crystals or nanophase separation of different refractive index compared to that of the glassy matrix [41].

X-Ray Powder Diffraction (XRDP) analysis was carried out on three different sections of the GC-fiber1 sample in accordance to the successive steps of the fiber drawing process. These are: (i) the formation of the drop and its stretching until attaining a fiber (approximate diameter ~200 µm), corresponding to the first stage of the drawing process; (ii) the drawing of the first meter of fiber while the parameters (furnace temperature, preform feeding rate and fiber tension) are being adjusted to achieve precisely the targeted diameter of 200 µm; and (iii) the controlled fiber drawing in stabilized conditions (fiber diameter of 200 µm). In Fig. 2, XRDP patterns of the three sections of the GC-fiber1 sample collected at each stage are presented. Both cell parameters and crystallite sizes were determined by Lebail refinements using a fundamental approach [42].

Optical Materials EXPRESS

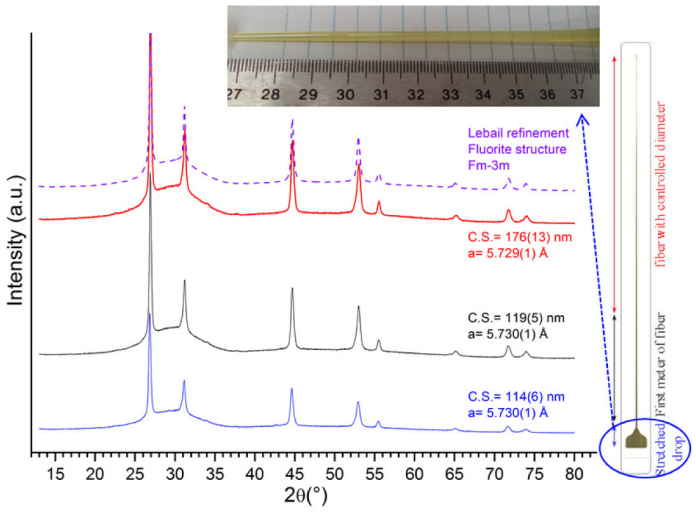

Fig. 2. XRPD patterns of sections of the GC-fiber1 sample collected at different stages of the fiber drawing from the glass preform shown in the curves from the bottom up: (i) in blue (bottom curve), from the stretched drop formed at the very beginning of the process. Inset photographs shows the drop stretched from the preform at 550 °C after a processing time of ~8-10 min; (ii) in black, from the first meter of the stretched fiber and (iii) in red, from the next 3-4 meters of pulled fiber (stable regime of drawing). The lattice parameters and the crystallite size were determined after refinement by using the Lebail method with fluorite structure as a starting model. a and C.S represents lattice parameter and crystal structure, respectively.

First, one can notice that a single fluorite crystalline phase can be identified in the drawn fibers. LeBail refinements performed from X-ray powder diffraction led to constant cell parameters for the three sections of fibers (a = 5.730(1) Å, Fm-3m space group). Compared to pure PbF_2 and CdF_2 fluorite crystalline phases exhibiting a = 5.94 Å [43] and a = 5.39 Å [44] cell parameters respectively, and given that the nominal composition is $30SiO_2–15Al_2O_3–27CdF_2–22PbF_2–4YF_3–2YbF_3$ (mol%), the crystalline phase can be considered as a mixed $Pb_{1-x-y-z}Cd_xY_yYb_zF_2$ fluorite phase. This is supported by the observation that the best match with reported structures in the ICDD database corresponds to a mixed $Pb_{1-x}Cd_xF_2$ phase [32, 33]. Furthermore, it is also well-known that *RE* elements easily substitute for Pb and Cd in the crystalline phase of glass-ceramics. As the $Pb_{1-x}Cd_xF_2$ cell parameters are expected to follow the Vegard's law between PbF_2 and CdF_2, a rough estimation of the fluorite composition could be $Pb_{0.7}(Cd,Y,Yb)_{0.3}F_2$, considering that ionic radii of Cd^{2+}, Y^{3+} and Yb^{3+} are similar [45]. However, it is difficult to precisely determine the cationic composition of the crystalline fluorite phase as the multiple cation composition prevents any Rietveld refinement to provide a clear answer.

A significant but expected variation of the crystallite size was observed along the drawing process. In the stretched drop, from XRD Lebail refinement, the crystal size (volume average) was determined to be about 114(6) nm (blue curve), which is consistent with the opalescence observed in the inset of Fig. 2. The crystallite size remains constant (119(5) nm) in the first meter of the drawn fiber. It eventually increases and reaches a value of about 176(13) nm once the process is stabilized, giving rise to about 3-4 meters of fibers with constant diameter and crystal size. To understand the crystal size evolution during the drawing process, three factors must be considered: (i) the preform feeding (vertical descent) into the drawing furnace, (ii) the temperature of the latter (i.e. the drawing temperature) and, (iii) the tension applied to the fiber while stretching. These parameters enable the fiber diameter and the drawing speed to be tailored. Here, to simplify our analysis, it can be reasonably stated that the uncontrolled crystallization observed in the stretched drop, the fiber and the residual preform is directly related to the thermal treatment applied on the material while drawing at 550°C (process duration ~8-10 to ~13-14 min).

Optical Materials EXPRESS

In the second method used to produce a $30SiO_2$-$15Al_2O_3$-$27CdF_2$-$22PbF_2$-$4YF_3$-$2YbF_3$ optical fiber, i.e. the crucible method or 'direct-melt process', pieces of fiber of about 1 m length were directly pulled out from the glass melt at a temperature of ~800-900°C. Such an approach, despite its limited control on the fiber diameter, enables perfectly vitreous optical fibers to be obtained, as shown in the corresponding XRPD pattern presented in Fig. 3. The heat-treatment performed at 460°C for 20h on some G-fiber2 sections led to the formation of $Pb_{1-x-y-z}Cd_xY_yYb_zF_2$ nanocrystals, i.e. the same phase as that observed in the GC-fiber1 samples, with similar lattice parameters (a = 5.74 Å). The diffraction peaks observed on the GC-fiber2 XRPD diffractogram in Fig. 3 appear broader than those observed in the XRPD pattern of the GC-fiber1 sample (Fig. 2). This information indicates the formation of smaller crystals, as confirmed by the volume average crystallite size of ~11.2(2) nm obtained by Lebail refinement method using a fundamental approach. Controlling the crystallization process from the glass fiber enables the fabrication of nanocrystals more than an order of magnitude smaller than those produced by preform drawing. Such a controlled crystallization is comparable to that already observed and largely investigated in the SiO_2-Al_2O_3-CdF_2-PbF_2-YF_3 system and derivate bulk samples [6].

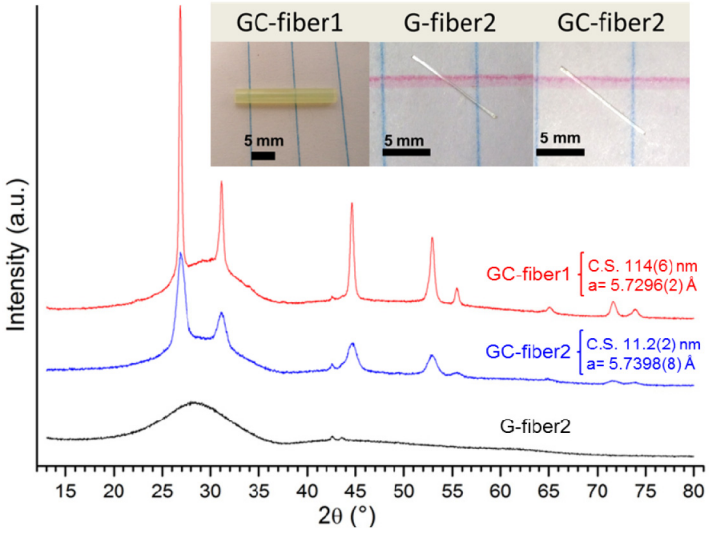

Fig. 3. XRPD diffraction patterns of the G-fiber2, GC-fiber2 and GC-fiber1 samples. GC-fiber2 was obtained by heat-treatment of G-fiber2 at 460 °C for 20h. GC-fiber1 was obtained by glass preform drawing at 550 °C. Lattice parameters and average volume crystallite size were determined by using the Lebail method. Inset: photograph of the fiber samples. The two small and sharp peaks located at 42.5 and 43.5° (2 theta) seem to be related to data collection but remain unexplained.

TEM analysis was performed on the G-fiber2 and GC-fiber2 samples, as presented in Fig. 4, respectively. From the presented micrographs and the respective electron diffraction patterns embedded, one can observe the amorphous nature of the G-fiber2 and a homogeneous distribution of nanocrystals within an amorphous matrix for the GC-fiber2 (Fig. 4). The presence of discrete diffraction rings with well-defined spots attests the good crystallinity of the material and match with the fluorite structure (a = 5.73 Å, Fm-3m). The average size of the crystallites (calculated from about 250 particles) is found to be 6.1 nm and the standard deviation is 2.1 (minimum and maximum sizes are 1.8 nm and 15.2 nm, respectively). The smaller average size observed by TEM compared to XRD Lebail refinements can be explained by the presence of a few larger particles (<10 nm) which have a large effect on the average volume size determined by XRD (TEM analysis provides a number average of crystallite sizes compared to XRD which provides a volume average of crystallite sizes).

Optical Materials EXPRESS

EDS analyses were performed with a 0.1nm probe size on both the glassy matrix and fluorite crystallites in order to confirm the $Pb_{1-x-y-z}Cd_xY_yYb_zF_2$ composition. Si, Al, Cd, Pb, Y and Yb cationic elements were quantified. Almost all of the Si was found to be located in the glass matrix. Special attention has been paid to the size of the crystallites (less than 10 nm) compared to the thickness of the sample analyzed by STEM-EDS (tens of nm in thickness). Most probably, some of the matrix was probed during crystallite EDS analysis resulting from the contribution of the glass matrix situated on top and/or below the crystallites. However, given the very low amount of SiO_2 detected in the crystallites and taking into account previous results in the literature [6], we have considered that all SiO_2 is contained in the glass matrix and all PbF_2 is contained in the crystallites. From these considerations, we were able to determine both the matrix composition and the composition of the crystallites. The glass matrix is therefore mainly composed of SiO_2 (86%) with 11% Al_2O_3 and 3% CdF_2. The proportion of Al_2O_3 is surprisingly very low compared to the nominal composition. As expected, Y and Yb cations were only detected in crystallites, leading to an average crystallite composition close to $60PbF_2 – 20CdF_2 – 12YF_3 – 8YbF_3$, corresponding to an average $Pb_{0.6}Cd_{0.2}Y_{0.12}Yb_{0.08}F_2$ crystalline phase composition. A significant Al_2O_3 content was detected at the level of the crystallite. The latter cannot be simply explained by the presence of the surrounding matrix situated above and/or below the crystallite given the matrix composition ($86SiO_2 – 11Al_2O_3 – 3CdF_3$). We stipulate that some Al_2O_3 might be located at the interface between the crystallites and the glass matrix, as observed in LAS systems [46]. On the other hand, the sum of CdF_2 content located both in the matrix and in the crystallites is lower than the CdF_2 nominal content. In fact, careful examination of STEM-EDX maps shows a clear Cd enrichment located in parts of some crystallites, which can explain the CdF_2 concentration difference (Fig. 4(d)). Contrary to TEM images which contrast result from crystalline areas (i.e. nanocrystals darker than the glass matrix), STEM-HAADF images exhibit crystallites with a brighter contrast than the matrix. The contrast observed in these micrographs is linked to the average Z or the density of the phases, which enable chemical contrast micrographs to be obtained. As the matrix is mainly composed of SiO_2 whereas the crystallites contain heavier elements (Cd, Pb, Y and Yb), the crystallites appear brighter on STEM-HAADF images.

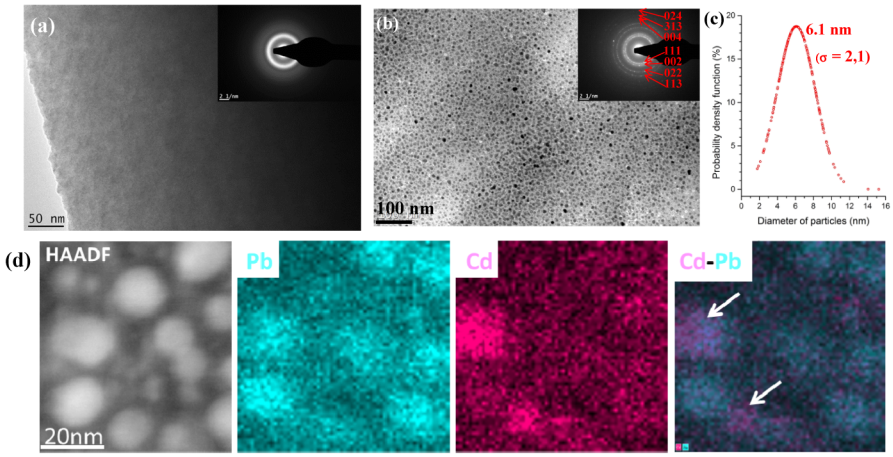

Fig. 4. (a) Bright field TEM micrograph of G-fiber2. The corresponding SAED pattern is embedded and shows the amorphous nature of the sample. (b) Bright field TEM micrograph of the GC-fiber2. The corresponding SAED pattern is embedded and shows the presence of nanometer scale crystals. (c) Size distribution and standard deviation (σ) of the crystallites in the GC-fiber2. (d) STEM-HAADF image and related EDS elemental maps for Pb, Cd and Pb-Cd in GC-fiber2. The overlaid EDS maps show the Cd local enrichment of certain parts on several crystallites (white arrows).

Optical Materials EXPRESS

In summary, the structural characterization carried out by XRPD and TEM on both glass-ceramic fibers have shown that: (i) the fluorite structure in both cases is $Pb_{1-x-y-z}Cd_xY_yYb_zF_2$ ($x + y + z \approx 0.3$-0.4) and with local variations of the Cd content, (ii) drawing fibers directly from the glass preform leads to uncontrolled crystallization with crystal sizes greater than 100 nm and varying along the fiber length, confirming that this fabrication method is inadequate here and; (iii) producing glass-ceramic fiber by appropriate and controlled heat-treatment of the parent glass fiber permits one to generate small nanocrystals (number-average size calculated as 6 nm by TEM and volume-average of 11 nm by XRD) with homogeneous size distribution and dispersion within the fiber, as well as larger crystal volume.

4.2. Optical characterization

The optical properties of the three samples of GC-fiber1, G-fiber2 and GC-fiber2 samples were investigated by means of photoluminescence (PL) under laser excitation at 975 nm. The recorded PL spectra are presented in Fig. 5(a). A higher PL intensity is obtained for the GC-fiber2 (heat-treated at 460 °C for 20h) than for its parent G-fiber2. Such a result was expected and can be explained by the progressive partition of Yb^{3+} ions into the fluorite $Pb_{1-x-y-z}Cd_xY_yYb_zF_2$ nanocrystals, decreasing the non-radiative relaxation rate and thus leading to an enhancement in the PL intensity. This effect was already largely investigated in *RE* ions doped glass-ceramics belonging to the SiO_2-Al_2O_3-CdF_2-PbF_2-YF_3 system or its derivatives [6]. GC-fiber1 exhibits lower PL intensity than G-fiber2 and GC-fiber2. This can be related to the formation of larger size crystals for GC-fiber1, as shown in Fig. 3, which can increase the scattering of emitted light and thus its reabsorption by the glass matrix (emission photon trapped within the sample). A red shift of the maximum emission peak from ~1005 to ~1020 nm is observed for the G-fiber2 and GC-fiber2 while the emission peak in the GC-fiber1 sample is also centered around 1020 nm.

The mean fluorescence wavelength [17], λ_F, is found to be 1010(1) nm, 1002(1) nm and 1008(1) nm for the GC-fiber1, G-fiber2 and GC-fiber2, respectively. In the following part, given the previously described PL properties, the results and discussion will be focused only on the G-fiber2 and GC-fiber2.

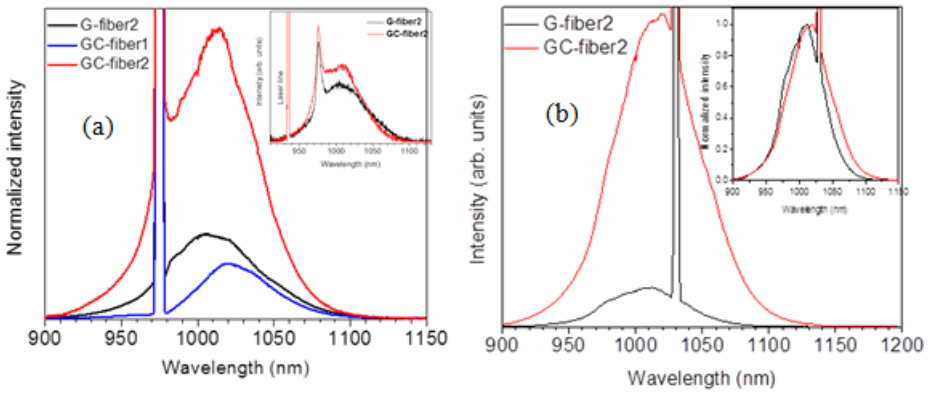

Fig. 5. (a) Normalized photoluminescence spectra (with respect to laser power) of the Yb^{3+}-doped GC-fiber1, G-fiber2 and GC-fiber2 upon 975 nm laser excitation. Inset: Absolute photoluminescence spectra of the G-fiber2 and GC-fiber2 samples upon 940 nm laser excitation. Both fibers are 10 mm long with a 200 µm diameter. (b) Anti-Stokes fluorescence spectra of the G-fiber2 and GC-fiber2 upon laser excitation at 1030 nm (400 mW power). Inset shows the same spectra after maximum intensity normalization for a better comparison.

Small pieces of G-fiber2 and GC-fiber2 of about 10 mm long were cut from a length of ~1 m as-drawn fibers. They were cleaved (with a fiber cleaver) on both ends prior to being used for absolute photoluminescence measurements performed with a method reported in a previous work [17]. The absolute PL spectra and photographs of the G-fiber2 and GC-fiber2 samples are shown in inset of Fig. 5(a). As expected, the PL intensity is higher in GC-fiber2

Optical Materials EXPRESS

than in G-fiber2 owing to the formation of a low phonon energy fluoride crystalline environment around the Yb^{3+} ions (i.e. $Pb_{1-x-y-z}Cd_xY_yYb_zF_2$ nanocrystals). The emission peak at 1005 nm in the G-fiber2 spectrum is slightly red shifted to about 1010 nm in the GC-fiber2 emission spectrum. Compared to G-fiber2, the emission band of GC-fiber2 sharpens and its tail at longer wavelengths is narrows, indicating a structuration of the surrounding of the Yb^{3+} ions.

The measured PLQY is 0.95(11) for GC-fiber2, which is larger than the values measured for G-fiber2 (0.83(11)) and reported for the bulk glass (0.92(11)) [46]. However, this value is slightly lower than that reported for bulk glass-ceramics (0.97(4)) with the same nominal composition and Yb^{3+} concentration [17]. Variations of PLQY between bulk and optical fibers may be ascribed to the use of samples of different dimensions and shapes which can affect the experimental error, particularly in the case of fibers.

To envisage the utilization of such fibers for applications in laser cooling, the fibers should fulfill specific requirements such as exhibiting anti-Stokes fluorescence. In Yb^{3+} doped materials, the cooling process is indeed based on anti-Stokes fluorescence (peaking around 1010 nm) after excitation with low energy photons in the range of 1030-1040 nm. The excited Yb^{3+} ions reach quasi-equilibrium with the lattice by absorption of a phonon. If the conversion process of phonons into anti-Stokes fluorescence is significantly high, the system starts to cool. Otherwise, the system simply heats [47]. The anti-Stokes fluorescence spectra measured on both G-fiber2 and GC-fiber2 upon laser excitation at 1030 nm are presented in Fig. 5(b). It appears clearly that a higher anti-Stokes fluorescence is obtained for the GC-fiber2 when compared to its parent G-fiber2. When both spectra are normalized to their maximum intensity, a red shift of the peak maximum and a red tail broadening are observed for the GC-fiber2 emission band, as shown in the inset of Fig. 5(b). Once again, this effect can be attributed to the incorporation of Yb^{3+} ions into the fluoride nanocrystals which is thus favorable in view of using the GC-fiber2 for applications in laser cooling.

It is worth mentioning that a bright blue up conversion emission (visible to the naked eye) was observed while performing the PL measurements upon 975 nm wavelength laser excitation of the fibers. Such a phenomenon is well-known and can be due either to a cooperative luminescence effect arising from Yb^{3+} ions [48], and/or an emission originating from other *RE* ions like Er^{3+} or Tm^{3+} (present as impurity traces) after energy transfer from Yb^{3+} ions [49]. To confirm the origin of this blue upconversion observed here, visible emission spectra were recorded by exciting the fibers with a 975 nm wavelength laser diode. The recorded emission spectra are presented in Fig. 6. As it can be seen, the visible emission bands observed from both G-fiber2 and GC-fiber2 can be attributed to radiative transitions of Er^{3+} and Tm^{3+} ions: at 410 nm from Er^{3+}: $^2H_{9/2}\rightarrow{}^4I_{15/2}$, at 478 nm from Tm^{3+}: $^1G_4\rightarrow{}^3H_6$, at 539 nm and 647 nm from Er^{3+}: $^2H_{11/2}$, $^4S_{3/2}\rightarrow{}^4I_{15/2}$ and $^4F_{9/2}\rightarrow{}^4I_{15/2}$, respectively. These transitions occur after energy transfer by APTE (addition photon transfer energy) effect from the Yb^{3+} ions which act as sensitizers. Such an effect is 10^5 times more efficient when compared with the cooperative luminescence for similar Yb^{3+}-Yb^{3+} interionic distance (in other words, for similar Yb^{3+} concentration) [48]. It is thus difficult to exclude the possibility of cooperative luminescence from Yb^{3+} ions here, as the latter can be hidden by the former. Nonetheless, one can reasonably state that the upconverted light emission observed in the G-fiber2 and GC-fiber2 samples essentially originates from the presence of Tm^{3+} and Er^{3+} contaminants whereas no Yb^{3+} ions clustering is expected in the crystals. Moreover, as no blue upconversion emission was observed in an undoped sample in the same conditions of laser excitation, one can conclude that the source of contamination is the ytterbium fluoride starting powder although a 99.99% (Alfa Aesar) purity chemical was used [34]. With respect to the laser cooling effect, it was recently shown in completely impurity-free systems (absence of Er^{3+} and Tm^{3+} ions) that cooperative luminescence has no influence [50]. However, as the demonstration of laser cooling was not successful at this stage of our studies on these nano-glass-ceramic fibers, we assume that the purity of the starting materials, not only of the Yb^{3+} precursor, but also of the other oxides and fluorides, is the primary limiting factor. Improving

Optical Materials EXPRESS

the starting materials purity by reducing their impurities (transition metal ions and OH^- groups) contents down to ppb levels is the key to achieve laser cooling.

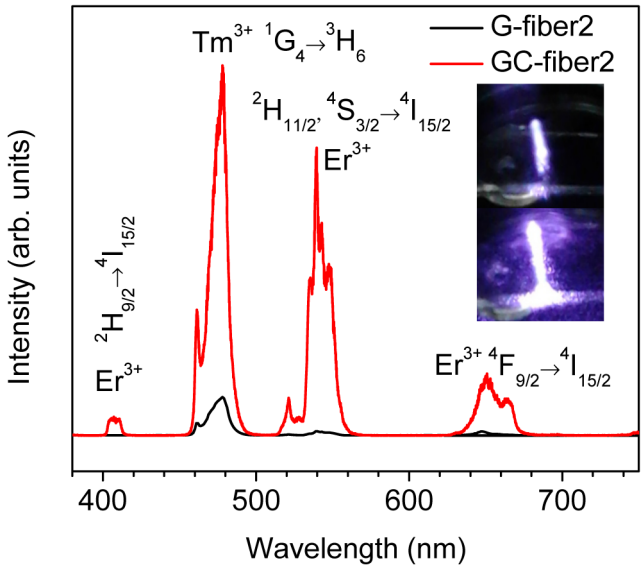

Fig. 6. Upconversion emission spectra of the G-fiber2 and GC-fiber2 samples upon laser excitation at 975 nm. The observed emission bands are ascribed to radiative transitions of the Tm^{3+} and Er^{3+} ions present as impurity traces in the material. Inset shows blue upconverted light emitted from the G-fiber2 (top) and GC-fiber2 (bottom) (diode power of 250 mW).

No cooling is expected to occur for the measured QE. With a 3% improvement in the QE, one should not expect cooling of the glass fibers, however, GC fibers would cool provided the background absorption is lower than 2 x 10^{-4} cm^{-1} [17], equivalent to 0.086 dB/m, without accounting for the segregation ratio. Our calculations show that this is an upper limit for the background absorption of the fibers so that cooling would be only possible for an enhanced QE of 0.98. On the other hand, the upper limit of the predicted background absorption using Eq. (1) for GC fibers is ~2.3 x 10^{-3} cm^{-1} (~1 dB/m), taking into account a segregation ratio of ~97% and with the following parameters: QE ~0.995 in nanocrystals as well as QE ~0.90 in glass matrix (GC consists of nanocrystal and glass matrices), volume fraction of nanocrystals ~50% and Yb^{3+} ion concentration, $N_T \approx 5 \times 10^8$ μm^{-3}. The upper limit of background absorption will change slightly with a change in Yb^{3+} ion concentration, QE, or the segregation ratio. Background attenuation measured in the fiber by the cut-back method gave a value of 15 dB/m. Although improvements in the fiber fabrication process should be pursued, the attenuation value does not mean that cooling cannot occur as it includes scattering, which does not necessarily lead to heating but just to transmission loss. A more representative and reliable technique to assess the background absorption would be a calorimetric method [17], which is not justified at the present time due to the fact that cooling is not yet expected for the fibers with QE below 0.98. However, our theoretical predictions show that the laser cooling effect is possible in this Yb^{3+}-doped SiO_2-Al_2O_3-CdF_2-PbF_2-YF_3 system, therefore it is anticipated that the demonstration of an experimental laser cooling will be realized soon. Work is currently ongoing to prepare ultra-high purity starting materials to reduce the material background absorption as well as improve the QE. In parallel, material fiber processing is also under development to produce longer Yb^{3+}-doped nano GC-fibers and step-index fibers as well to ensure efficient light confinement and guiding.

Optical Materials EXPRESS

5. Conclusions

Ytterbium-doped single-index glass-ceramic optical fibers were successfully produced by two methods: (i) by conventional drawing from a glass preform and, (ii) by the crucible technique ('direct-melt process') followed by controlled heat-treatment. It was demonstrated that heat-treating the parent glass-fiber is preferable to conventional glass preform drawing to produce nano-glass-ceramic fibers with nanocrystals homogeneously distributed along the fiber. XRPD and TEM analyses have evidenced the formation of $Pb_{1-x-y-z}Cd_xY_yYb_zF_2$ ($x + y + z \approx 0.3$-0.4) small nanocrystals (number-average size of 6 nm by TEM and volume-average of 11 nm by XRD) with small distribution of shape and size, dispersion within the fiber, as well as larger crystal volume. On the other hand, the preparation of GC-fiber by glass preform drawing did not allow a fine tailoring of the crystallization process and *in fine* of the crystals size, shape and distribution along the fiber. Nevertheless, efforts must be devoted to improve the 'direct-melt' drawing process to produce longer fibers with constant diameter.

Photoluminescence studies upon laser excitation at wavelengths of 940 and 975 nm confirm a significant enhancement of the Yb^{3+} luminescence intensity for the nano-GC-fiber (heat-treated at 460 **°C** for 20h) when compared to the vitreous G-fiber and the GC-fiber (obtained by preform drawing). Upon laser excitation at a wavelength of 1030 nm, higher anti-Stokes fluorescence intensity was obtained for the GC-fiber when compared to its parent glass-fiber. The photoluminescence quantum yield (PLQY), determined upon laser excitation at 940 nm, is also significantly higher (95%) for the nano GC-fiber. Moreover, from our simulations, it appears clearly that the nano GC-fiber can exhibit laser cooling effect if a segregation ratio (~95%) of Yb^{3+} ions within the fluoride nanocrystals to achieve PLQY close to unity. Last, the presence of Er^{3+} and Tm^{3+} ions as contaminants has been revealed, even though high purity 99.99% starting materials were used.

In summary, this study has demonstrated the potential for using Yb^{3+}-doped SiO_2-Al_2O_3-CdF_2-PbF_2-YF_3 nano-glass-ceramic fibers in laser cooling applications, although this effect was not yet clearly evidenced. The theoretical calculations and better understanding of material processing reported here pave the way for future developments where improving the chemical purity and producing longer (step-index) nano-glass-ceramics fibers will constitute the main challenges that need to be addressed.

Funding

Natural Sciences and Engineering Research Council of Canada (NSERC), the Canadian Excellence Research Chair program (CERC) on Enabling Photonic Innovations for Information and Communication, the Canada Research Chairs program on Future Photonics Systems, the Canadian Natural Sciences and Engineering Council's Discovery and Strategic Grants programs. The authors are also grateful to the Fonds Québecois de la Recherche sur la Nature et les Technologies (FQRNT) for the financial support and the Canada Foundation for Innovation (CFI) for infrastructure support. The authors thank Ye-Jin Yu for helping in the measurements at École Polytechnique Montréal and the French laboratory Interfaces, Confinement Matériaux et Nanostructure (ICMN, UMR-CNRS 7374) based in Orléans for TEM access. We thank ANR for its financial support to the project FOCAL ANR-14-CE07-0002.